Antibacterial Activity of Solid-Supported Gold Nanorods Combined with Antimicrobial Peptides

Downloaded from: https://research.chalmers.se, 2026-07-14 09:37 UTC

Citation for the original published paper (version of record):
Lidström Uusitalo, M., Nilsson, A., Schäfer, A. et al (2026). Antibacterial Activity of Solid-Supported Gold Nanorods Combined with Antimicrobial Peptides. ACS APPLIED BIO MATERIALS, In Press. http://dx.doi.org/10.1021/acsabm.6c00525

N.B. When citing this work, cite the original published paper.

research.chalmers.se offers the possibility of retrieving research publications produced at Chalmers University of Technology. It covers all kind of research output: articles, dissertations, conference papers, reports etc. since 2004. research.chalmers.se is administrated and maintained by Chalmers Library

(article starts on next page)

ACS APPLIED BIO MATERIALS

Open Access

This article is licensed under CC-BY 4.0

www.acsabm.org

Article

Antibacterial Activity of Solid-Supported Gold Nanorods Combined with Antimicrobial Peptides

Published as part of ACS Applied Bio Materials special issue "Antimicrobial and Antibiofilm Biointerfaces".

Maja Lidström Uusitalo, Alva Nilsson, Ann-Britt Schäfer, Gustav Eriksson, Mats Hulander, Michaela Wenzel, and Martin Andersson*

Cite This: https://doi.org/10.1021/acsabm.6c00525

Read Online

ACCESS | Metrics & More | Article Recommendations | Supporting Information

ABSTRACT: In response to the growing clinical challenge of combating biomaterial-associated infections (BAIs), antibacterial modifications of biomaterials have emerged as a promising alternative. One approach harnesses the photothermal properties of plasmonic nanoparticles to achieve a light-activated antibacterial activity through localized heating. This study evaluates a combined antibacterial strategy based on the photothermal heating of solid-supported gold nanorods and the antimicrobial peptide (AMP) RRPRPRPRPWWWW-NH_2. The antibacterial activity of the solid-supported gold nanorods under near-infrared (NIR) irradiation and of the AMP was evaluated individually and in combination against *Staphylococcus aureus*. Combining the photothermal heating of the gold nanorods with the AMP resulted in an enhanced antibacterial efficacy, achieving 98% reduction compared to the untreated control. Interestingly, the material characteristics and irradiation parameters governing the photothermal heating strongly influenced the activity of the combined system. This effect was observed even at low gold nanorod surface coverage (~15%), largely preserving the inherent surface properties of the biomaterial. Additionally, bacterial cytological profiling provided insight into the mode of action of the solid-supported gold nanorods and the AMP. The findings highlight key characteristics of this combined antibacterial strategy that are relevant for the development of improved biomaterials to combat BAIs.

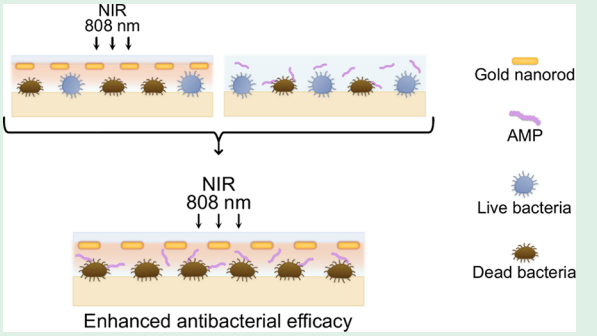

KEYWORDS: *gold nanorods, antimicrobial peptides, photothermal therapy, near-infrared light, biomaterial-associated infections*

Downloaded via 155.4.128.246 on June 26, 2026 at 14:34:17 (UTC).
See https://pubs.acs.org/sharingguidelines for options on how to legitimately share published articles.

1. INTRODUCTION

The development of antibacterial modifications of biomaterials has emerged over recent decades as a promising response to the significant clinical challenge posed by biomaterial-associated infections (BAIs). BAIs originate from bacterial adhesion to the biomaterial surface, which, following bacterial proliferation and biofilm formation, develop into hard-to-treat infections. The severity of these infections stems from the ability of biofilm-growing bacteria to evade the immune response and from their high tolerance to conventional antimicrobial agents like antibiotics.[1] The issue is further complicated by the increasing occurrence of antimicrobial-resistant pathogens,[2,3] rendering progressively more treatment options ineffective. In the development of antibacterial modifications of biomaterials, the aim is to provide the biomaterial itself with antibacterial properties, thereby enabling local prevention or treatment of infections. A range of strategies has been employed for this purpose, including making anti-adhesive surfaces that prevent initial bacterial colonization, as well as contact-killing or drug-eluting surfaces that actively eradicate bacteria on and in the immediate vicinity of the biomaterial.[4,5]

One type of antibacterial modification strategy utilizes the photothermal properties of plasmonic nanoparticles by immobilizing them onto the material surface, thereby obtaining a light-activated antibacterial effect through localized emission of heat.[6] A common choice of plasmonic nanoparticle is gold nanorods, owing to their tunable plasmon resonance frequency in the near-infrared (NIR) region known as the first biological window (750–900 nm).[7] Light within this frequency range exhibits optimal tissue penetration[8] and thus enables extracorporeal excitation and heat generation. Several studies, including previ-

Received: March 19, 2026
Revised: May 27, 2026
Accepted: May 28, 2026

ACS Publications

© XXXX The Authors. Published by American Chemical Society

ous work from our research group, have demonstrated a strong, broad-spectrum antibacterial activity of materials based on solid-supported gold nanorods,[9−12] highlighting their potential as an alternative or complement to conventional treatment of BAIs. For these systems, the antibacterial activity is commonly attributed to membrane disruptive effects caused by the photothermal heating.[13−15] However, little is known about how the antibacterial activity of these materials is influenced by the presence of antimicrobial compounds in suspension. Since systemic administration of antibiotics is common in the management of BAIs, for example, as preoperative prophylaxis and in treatment of prosthesis-related infections,[16] understanding the combined antibacterial effect is of high relevance.

With many conventional antibiotics losing their efficacy due to the increased occurrence of antimicrobial-resistant pathogens, there is a growing interest in alternative classes of antimicrobial compounds, one of which is antimicrobial peptides (AMPs). AMPs constitute an essential component of the innate immune defense of most multicellular organisms and have garnered considerable attention as alternatives to antibiotics owing to their broad-spectrum activity against bacteria, viruses, and fungi.[17,18] Their activity is attributed to some key structural features, including a small size, net cationic charge, amphipathic nature, and ability to form defined secondary structures.[18] The bacterial targeting ability of AMPs stems primarily from their net cationic charge, enabling electrostatic interaction with anionic moieties on the bacterial envelope.[17] This electrostatic interaction, together with the amphiphilicity of AMPs, can induce disruption of the bacterial membrane integrity. However, the mode of action of AMPs is not restricted to such membrane-disruptive mechanisms as they may also target cell-internal processes like cell division, DNA or RNA synthesis, and protein folding.[18]

Enhanced antibacterial activity has been reported when combining AMPs with photothermal heating from gold nanorods, both for AMPs functionalized onto the nanoparticles,[19−22] and where AMPs and gold nanorods are co-dispersed within a hydrogel matrix.[23] Thus, combining the bactericidal effect of AMPs with the photothermal heating of solid-supported gold nanorods presents a promising strategy for combatting BAIs. In the present study, we evaluated the antibacterial activity of photothermal heating generated from solid-supported gold nanorods combined with the cationic AMP RRPRPRPRP WWWW-NH_2 (RRP9W4N). This AMP has previously been employed by our research group for covalent attachment onto hydrogels, producing materials with prominent broad-spectrum antibacterial activity.[24−28] In addition, this work investigated the mechanisms underlying the antibacterial activity of this combined system by studying the interaction between the gold nanorods and the bacteria cells using electron microscopy, as well as assessing the mode of action through bacterial cytological profiling.[29]

2. RESULTS AND DISCUSSION

2.1. Material Characterization

In this study, two populations of gold nanorods were evaluated. From the Vis-NIR absorption spectra of the gold nanorod suspensions, shown in Figure 1A, the longitudinal plasmon resonance peaks of the gold nanorods were determined to be 840 and 870 nm, respectively. To distinguish between the two gold nanorod populations, they are hereafter referred to as AuNR840 and AuNR870. In Figure 1A, the position of the employed 808 nm NIR laser is also indicated, showing the extent of overlapping with the resonance bands of the respective nanorod

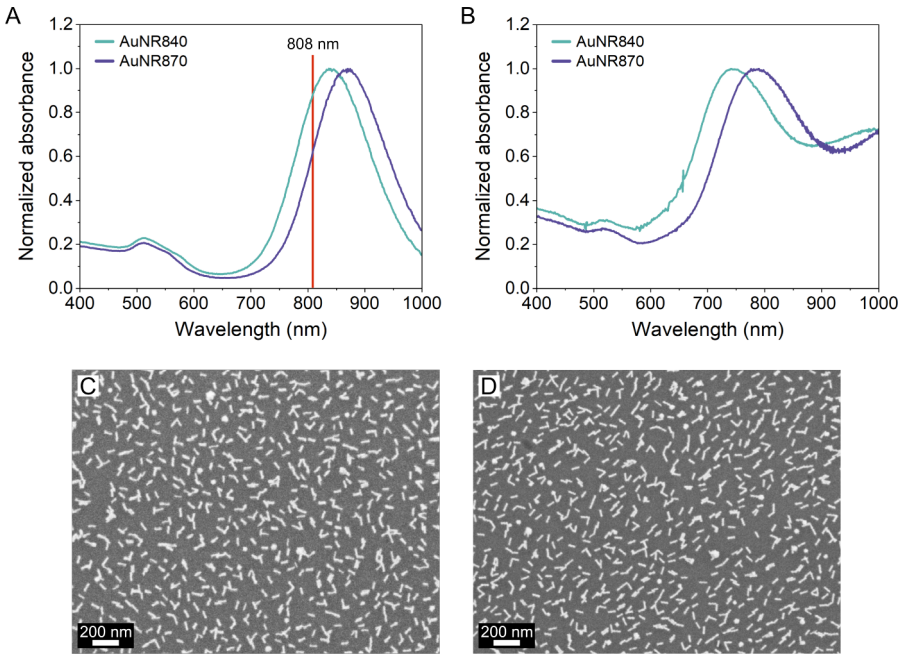

Figure 1. (A) Normalized Vis-NIR absorption spectra of the two populations of gold nanorods (AuNR840 and AuNR870) in aqueous suspensions, showing the longitudinal resonance peaks at 840 and 870 nm, respectively. (B) Vis-NIR absorption spectra of AuNR840 and AuNR870 supported on glass substrates, measured in air. SEM micrographs of (C) AuNR840 and (D) AuNR870 supported on glass substrates, showing the uniform distribution of nanorods on the substrate surfaces.

https://doi.org/10.1021/acsabm.6c00525
ACS Appl. Bio Mater. XXXX, XXX, XXX−XXX

populations. In previous work by our group, TEM analysis has been performed for gold nanorods synthesized using a corresponding synthesis procedure, with slight variations of the concentrations to tune the aspect ratio of the nanorods, showing their rod-like nanostructure and fcc single-crystalline nature.[30] A TEM micrograph of gold nanorods synthesized with the same procedure as AuNR870 is shown in Figure S1. Additionally, our group has published work where the properties of the solid-supported gold nanorods were studied in detail with XRD, showing their single-crystalline characteristics and the strong orientation of the nanorods on the support, as well as studying their photothermal characteristics under NIR irradiation.[30,31]

The gold nanorods were surface-attached to glass substrates, and the materials were characterized by Vis-NIR spectroscopy and scanning electron microscopy (SEM). The Vis-NIR absorption spectra of the gold nanorods supported on glass, measured in air, are shown in Figure 1B, where the retention of the two characteristic plasmon resonance peaks can be observed. The blue-shift of the longitudinal peaks from 840 nm and 870 nm to 740 nm and 790 nm, respectively, is caused by the difference in refractive index of the medium surrounding the nanorods, transitioning from water to the glass-air interface. SEM micrographs of AuNR840 and AuNR870 supported on glass are shown in Figure 1C,D, respectively, demonstrating a uniform distribution of nanorods over the substrate surface. The surface coverage of gold nanorods was determined through image analysis of SEM micrographs as the projected area covered by particles. The AuNR840 samples exhibited a surface coverage of 13%, while the AuNR870 samples had a surface coverage of 15%.

To estimate the temperature increase upon NIR irradiation of the solid-supported gold nanorods, the photothermal heating was evaluated using thermal imaging. AuNR840 and control (bare glass) samples were placed onto Mueller–Hinton agar plates, and thermal images were recorded before and after 30 s NIR irradiation at 4.7 W cm^{-2}. The results are shown in Figure S2. Based on the thermal imaging, the average temperature increase ($n = 3$) for the solid-supported gold nanorod samples was approximately 30 °C, reaching a maximum temperature around 55 °C, whereas the glass control samples exhibited an increase of about 2 °C under identical irradiation conditions.

2.2. In Vitro Antibacterial Activity

The in vitro antibacterial activity against *Staphylococcus aureus* (CCUG 10778) was evaluated using an agar plate model, adapted from a previously described protocol.[9] The antibacterial activity of the solid-supported AuNR840 and AuNR870 samples upon NIR irradiation for 30 s at 4.7 and 5.4 W cm^{-}, respectively, in the absence and presence of 3.125 μM RRP9W4N AMP, is shown in Figure 2A. Bare glass samples were used as controls. Representative images of the samples from the agar plate model are shown in Figure 2B. The NIR laser intensities employed for AuNR840 and AuNR870 were adapted to achieve comparable antibacterial efficacy, wherein a higher intensity was used for the AuNR870 samples, which exhibited lower absorbance at 808 nm (Figure 1A).

The minimum inhibitory concentration (MIC) of RRP9W4N against *S. aureus* CCUG 10778 has previously been determined to be in the range of 6–12 μM.[28,32] In the present study, a sub-MIC concentration of 3.125 μM was employed, which resulted in a significant antibacterial activity, corresponding to an antibacterial efficacy of 68% relative to the untreated control, without completely inhibiting bacterial growth. Both AuNR840 and AuNR870 samples demonstrated significant antibacterial activity upon NIR irradiation, attributed to the photothermal heating of the gold nanorods, yielding antibacterial efficacies of 89 and 88%, respectively, relative to the untreated control. Moreover, the bactericidal effect from the photothermal heating of both populations of solid-supported gold nanorods was significantly greater than that observed for RRP9W4N alone. Additionally, when comparing the antibacterial activity of RRP9W4N alone with the activity when combined with NIR light, no significant differences were detected (Figure S3). As such, the slight temperature increase caused by NIR irradiation in the absence of gold nanorods (around 2 °C, Figure S2) did not enhance the antibacterial activity of RRP9W4N.

Importantly, the gold nanorods did not affect bacterial viability in the absence of NIR light, and the NIR light alone showed no effect in the absence of the gold nanorods (Figure S3). Both observations are consistent with the results reported in our previous publication investigating similar solid-supported gold nanorod materials.[9] In this previous study, it was also demonstrated through SEM analysis that the gold nanorod-functionalization remained largely unaffected after the in vitro antibacterial activity evaluation. This indicates that the gold nanorods have a good stability on the glass substrates. However, as the long-term stability is a critical parameter for the potential clinical translation of the materials, these aspects

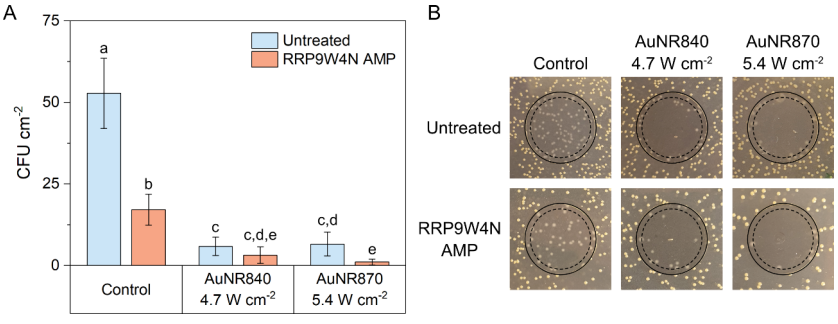

Figure 2. (A) Antibacterial activity against *S. aureus* (CCUG 10778) of solid-supported AuNR840 and AuNR870 on glass, irradiated with NIR light for 30 s at 4.7 and 5.4 W cm^{-}, respectively. Blue bars represent untreated bacterial suspension, and orange bars represent the presence of 3.125 μM RRP9W4N. Data are presented as the average CFU cm^{-2} for nine samples ($n = 9$) and the error bars denote standard deviation. Statistical significance was determined with pairwise two-sample *t*-tests assuming unequal variance. Significance level: $p < 0.05$. (B) Example pictures of the samples from the agar plate model. The black solid lines indicate the samples' perimeter, and the dashed lines encircle the sampling area.

https://doi.org/10.1021/acsabm.6c00525
ACS Appl. Bio Mater. XXXX, XXX, XXX–XXX

should be investigated in substantially greater detail in future studies.

When studying the combined effect of NIR-irradiated solid-supported gold nanorods and RRP9W4N, the results diverged between the AuNR840 and AuNR870 samples. For AuNR840 irradiated at 4.7 W cm^{-2}, no significant enhancement of the antibacterial activity was observed in the presence of RRP9W4N (Figure 2A). In contrast, for AuNR870 irradiated at 5.4 W cm^{-2}, a significant increase in the antibacterial activity was demonstrated in the presence of RRP9W4N. Specifically, in the presence of 3.125 μM RRP9W4N, the antibacterial efficacy of the NIR-irradiated AuNR870 samples increased from 88 to 98%. Similar to what has been shown for AMP-functionalized gold nanorods in suspension,[19−22] it appears that the antibacterial efficacy can be enhanced when combining the photothermal heating from the solid-supported gold nanorods with RRP9W4N. However, the specific material characteristics and laser irradiation parameters that determine the extent of photothermal heating are critical in such a combined system, as demonstrated by the divergence of the results between the AuNR840 and AuNR870 samples. These findings clearly illustrate the importance of controlling both the gold nanorod synthesis, which determines the nanorod size, shape, and aspect ratio, and the surface attachment, which together governs the plasmonic properties that, in turn, influence the magnitude of the combined antibacterial effect of the solid-supported gold nanorods with the AMP.

2.3. Interaction between Gold Nanorods and *S. aureus*

To investigate the interaction between the solid-supported gold nanorods and *S. aureus* in the absence of NIR light, electron microscopy was used. Titanium substrates were employed in these investigations owing to their superior conductivity compared to glass, and the samples had a gold nanorod surface coverage of 10%. A monolayer of *S. aureus* was cultured on the surfaces, and following fixation, bacterial attachment was visualized using SEM. As seen in Figure 3A, the cells resembled hard spheres resting on the surface with limited physical contact, surrounded by gold nanorods evenly distributed on the surface. The small contact area between the cells and the substrate found during SEM analysis was confirmed with TEM analysis. TEM micrographs at different magnifications showing cross sections of the interaction between AuNR870 on titanium and *S. aureus* are shown in Figure 3B–D. The dark layer covering the bacterial cells corresponds to a 100 nm chromium layer, sputter coated to protect the surface during TEM specimen preparation, while the irregularities visible in the center of the cells are likely artefacts caused by damage from the high-voltage electron beam. As no contrasting agents were used in the TEM specimen preparation, no internal cell structures are visible.

TEM micrographs revealed that the cross section of the contact area between the bacterial cells and the material surface was limited to the order of a few hundred nanometers. Based on the micrographs, it is reasonable to assume a circular contact area with a diameter in the range of 100–300 nm, which corresponds to each cell being in contact with 1–8 gold nanorods (details are provided in the Supporting Information). Surprisingly, despite the low number of nanoparticles in direct contact with the bacteria, the gold nanorods exhibited strong antibacterial activity upon NIR irradiation (Figure 2), highlighting the efficiency of this photothermal approach. However, it should be noted that

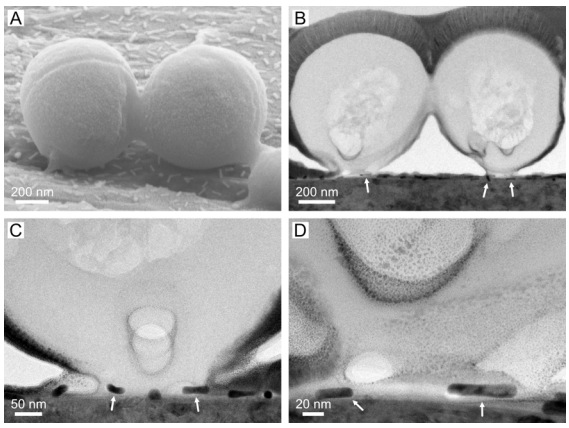

Figure 3. Electron microscopy study of the interaction between gold nanorods supported on titanium and *S. aureus*. (A) SEM micrograph visualizing two *S. aureus* cells on AuNR870. (B–D) TEM micrographs at different magnifications showing the interaction between the bacterial cells and the gold nanorods, with (D) showing a higher magnification of the interface of the leftmost bacterial cell in (B). The dark top layer represents the sputtered 100 nm chromium coating, and the lighter circular structures represent bacterial cells in cross section. No intracellular structures are visible, as the TEM specimen preparation was conducted without the use of contrasting agents. The dark ellipsoids beneath the bacteria correspond to the supported gold nanorods, indicated by white arrows at selected locations.

biological specimens are known to deform or shrink during preparation for electron microscopy and that the actual contact area could be slightly underestimated.[33] Nonetheless, these findings highlight the potential of this system as an antibacterial modification strategy that minimizes influence on the biomaterials' innate surface characteristics. This is of relevance as biomaterial surfaces are typically designed to interact favorably with the biological environment in which they are intended to function. Together with the localized antibacterial activity of the NIR-irradiated solid-supported gold nanorods, demonstrated by the ability of bacteria to recolonize the samples from regions outside the irradiated area (Figure 2B), these findings show promise for minimizing adverse effects on surrounding tissue cells. However, to fully evaluate the biocompatibility of the proposed antibacterial surface modification strategy, further in vitro studies using eucaryotic cells, and preferably also in vivo studies, are required.

2.4. Bacterial Cytological Profiling

To gain insight into the mode of action of AuNR840 in combination with RRP9W4N, we employed bacterial cytological profiling (BCP), a phenotypic analysis method that allows the assessment of several cell parameters in a single assay. In this study, we used a BCP variant that combines four specific fluorescent dyes: DAPI to visualize DNA, SytoxGreen to assess membrane integrity, FM4-64 to visualize changes in membrane morphology, and $DiSC_35$ to assess the membrane potential.[29,34] *S. aureus* (CCUG 10778) was exposed to AuNR840 alone, in combination with RRP9W4N, or together with the pore-forming antibiotic nisin, which serves as a positive control in the assay.[34,35] Samples were subsequently irradiated with NIR light at an intensity of 4.7 W cm^{-2} for 30 s or left untreated as controls.

https://doi.org/10.1021/acsabm.6c00525
ACS Appl. Bio Mater. XXXX, XXX, XXX−XXX

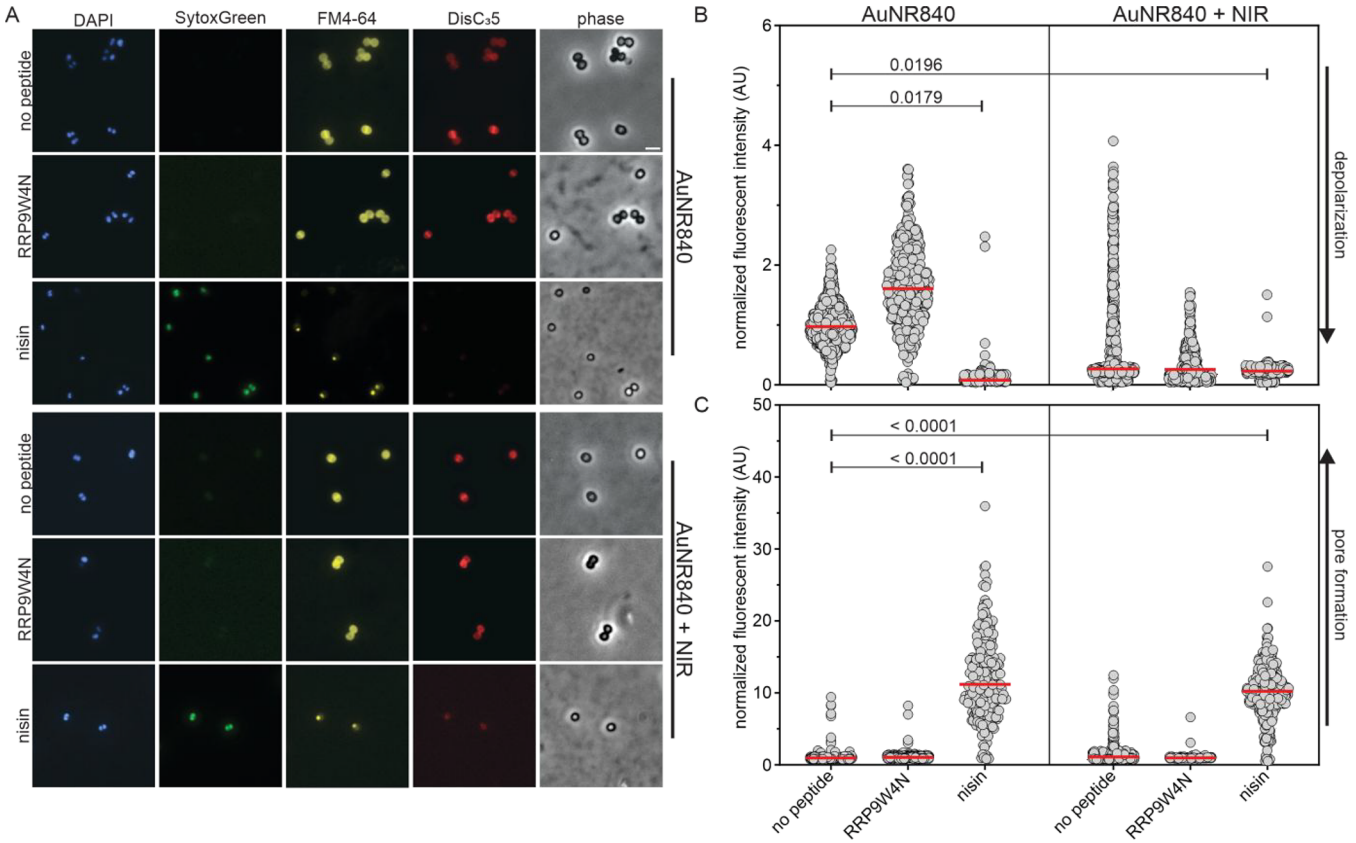

Figure 4. Bacterial cytological profiling of *S. aureus* (CCUG 10778) treated with AuNR840, AuNR840 treated with RRP9W4N, or AuNR840 combined with nisin, with or without exposure to NIR light at an intensity of 4.7 W cm^{-2} for 30 s. (A) Treated cells were transferred to agarose patches containing DAPI for DNA staining, SytoxGreen to report large membrane pores, FM4-64 for staining cell membranes and visualizing changes to membrane morphology, and $DiSC_35$ to report membrane potential. Scale bar is 2 μm. (B) Quantification of $DiSC_35$ fluorescence from microscopy images. $DisC_35$ is a voltage-sensitive dye that accumulates in cell membranes with an intact membrane potential. If cells depolarize, the dye dissociates from the membrane, resulting in a decrease in fluorescence signal.[36] The graph shows pooled data from three biological replicates. Red lines indicate the median. Statistical significance was determined using a one-way nested ANOVA. (C) Quantification of SytoxGreen uptake from microscopy images. SytoxGreen is a DNA-binding dye that does not penetrate intact membranes; however, upon formation of membrane pores large enough to allow passage of the molecule, it diffuses into cells, producing a bright DNA signal.[37,38] The graph shows pooled data from three biological replicates. Red lines indicate the median. Statistical significance was determined with a one-way nested ANOVA.

Both non-irradiated and irradiated samples treated with the AuNR840 and nisin combination showed characteristic phenotypes indicative of membrane pore formation. Thus, cells appeared smaller and less phase-dense in phase contrast images (Figures 4A, S3B,C), showed clear FM4-64 foci representing membrane domain formation (Figure 4A), displayed strongly reduced $DisC_35$ fluorescence consistent with membrane depolarization (Figure 4A,B), and demonstrated clear SytoxGreen uptake, confirming the occurrence of large membrane pores (Figure 4A,C).

In contrast, the samples exposed to AuNR840 alone or in combination with RRP9W4N showed no evidence of major membrane disruption, either with or without NIR exposure. Cells showed no signs of cell lysis in phase contrast images and appeared similarly sized and phase-dense as cells exposed to AuNR840 alone without irradiation (Figures 4A, S4B,C). Consistent with this, cells showed no SytoxGreen uptake and no membrane aberrations in the FM4-64 staining (Figure 4A,C). This finding was surprising, as previous studies on RRP9W4N have shown membrane disruption, albeit at a much higher concentration of 30 μM (2.5 to 5-fold MIC).[39] These observations led us to hypothesize that lower concentrations of RRP9W4N, while still bactericidal, do not induce pore formation but rather act through an alternative mechanism. Interestingly, both non-irradiated and irradiated samples treated with RRP9W4N showed a reduction in DAPI intensity (Figure S4A), a phenotype typically associated with DNA damage and nucleoid fragmentation.[40,41] Although this requires further assessment in future studies, it is conceivable that the addition of the AMP adds a DNA-damaging component to the overall mode of action.

Furthermore, a heterogeneous depolarizing effect was observed in the NIR-irradiated samples exposed to AuNR840 alone and in combination with RRP9W4N; however, this effect was not statistically significant due to high variability between biological replicates (Figure 4A,B). This trend may indicate that the photothermal heating caused by the NIR irradiation of AuNR840, with and without RRP9W4N, can affect the cell membrane to some extent without inducing membrane pore formation. This interpretation is supported by previous studies, which have shown that the photothermal heating of solid-supported gold nanorods[14,15] and of gold nanorods in

https://doi.org/10.1021/acsabm.6c00525
ACS Appl. Bio Mater. XXXX, XXX, XXX–XXX

suspension[22,42,43] can cause membrane-disruptive effects on bacterial cells. Nevertheless, additional studies are required to validate and clarify the specific impact on membrane integrity.

3. CONCLUSIONS

This study explored the combined antibacterial activity of the photothermal heating generated by the solid-supported gold nanorods together with the AMP RRP9W4N. Upon NIR excitation, the solid-supported gold nanorods demonstrated a significant bactericidal effect against *S. aureus*, despite the low number of nanorods in direct contact with the bacterial cells. When the photothermal heating of the solid-supported gold nanorods was combined with RRP9W4N, enhanced antibacterial efficacy was demonstrated, depending on specific material characteristics and laser power. Investigation of the mode of action of NIR-irradiated solid-supported gold nanorods and RRP9W4N using bacterial cytological profiling revealed that the treatments did not cause major membrane disruption, either individually or in combination. The RRP9W4N AMP showed indications of causing DNA damage, whereas NIR-irradiated solid-supported gold nanorods produced a heterogeneous membrane depolarizing effect.

The proposed approach serves as an on-demand antibacterial strategy that can be externally controlled through NIR irradiation, which minimizes exposure of surrounding tissues to antimicrobial stress and provides spatial and temporal control. The pronounced antibacterial activity demonstrated for the relatively low surface coverage of gold nanorods highlights the efficiency of this photothermal approach, where bacterial inactivation is primarily achieved through thermal damage. The dual-action strategy realized by combining the photothermal heating of the gold nanorods with the AMP demonstrated a significant enhancement of the antibacterial effect, originally hypothesized to stem from the fact that both components target the bacterial envelope. However, the findings from the BCP study suggested a more multifaceted mode of action, involving several concurrent membrane-associated and intracellular stress responses, rather than solely pore formation. Altogether, the findings of this study provide initial insight into the mode of action of this combined system and demonstrate the potential of using photothermal gold nanorods in combination with AMPs to obtain an effective antibacterial modification strategy for biomaterials while minimizing alteration of the original material surface characteristics.

4. EXPERIMENTAL SECTION

4.1. Gold Nanorod Synthesis

Gold nanorods were synthesized according to a previously published procedure[9,30] based on a protocol by Scarabelli et al.[44] In brief, a gold seed suspension was prepared in a 30 °C water bath by mixing 4.7 mL of 100 mM hexadecyltrimethylammonium bromide (CTAB) solution with 25 μL of 50 mM gold(III) chloride ($HAuCl_4$) solution. Once the mixture was homogeneous, 300 μL of 10 mM sodium borohydride solution was added under vigorous stirring. The prepared seed suspension was then kept at mild stirring at 30 °C until use. For the gold nanorods with a longitudinal resonance peak at 840 nm (AuNR840), a growth solution was prepared in a 30 °C water bath by mixing 60 mL of 100 mM CTAB solution with 1.14 mL of 1 M hydrochloric acid solution and 600 μL of 50 mM $HAuCl_4$. After stirring for approximately 10 min, 720 μL of 8 mM silver nitrate solution was added, followed by 600 μL of 110 mM L-ascorbic acid solution. For gold nanorods with a longitudinal resonance peak at 870 nm (AuNR870), the growth solution was prepared correspondingly, except that the silver nitrate concentration was adjusted to 10 mM and the ascorbic acid concentration to 100 mM. Finally, 144 μL of the prepared seed suspension was added to the growth solution, thoroughly mixed, and then left undisturbed at 30 °C for 1 h and 50 min. The synthesized gold nanorods were purified by three successive centrifugations with redispersion in ultrapure water.

4.2. Surface Attachment of Gold Nanorods

Gold nanorods were attached to the surface of glass substrates (round coverslips, #1.5, 13 mm diameter, VWR) according to previously published protocols.[9,30] This attachment relies on electrostatic interactions between the cationic gold nanorods, which commonly have a zeta potential of around 30–50 mV depending on the CTAB concentration in the surrounding suspension,[9,45] and an anionic glass substrate. Briefly, the glass substrates were rinsed with ethanol (95%) followed by ultrapure water and then dried in a flow of nitrogen gas. The substrates were subsequently immersed in concentrated nitric acid (65–67%) overnight (18–19 h). The following day, the substrates were thoroughly rinsed with ultrapure water before being immersed in a gold nanorod suspension for 5 h, allowing for the electrostatic attachment of the cationic, CTAB-stabilized gold nanorods to the anionic glass surface. The as-prepared gold nanorod suspensions were diluted with ultrapure water to reach an absorbance of 0.35 at 400 nm. After 5 h, the gold nanorod suspension was exchanged to ultrapure water, after which the samples were immersed in ethanol (99.5%) and allowed to air dry. For the investigations of the interactions between the solid-supported gold nanorods and the *S. aureus* bacterial cells using electron microscopy, the AuNR870 were attached to titanium substrates (9 mm diameter, 2 mm thickness). The titanium samples were prepared similarly to the glass samples, except that instead of immersion in nitric acid, the titanium substrates were cleaned by UV/O_3 treatment for 15 min prior to immersion in the AuNR suspension.

4.3. Characterization of Solid-Supported Gold Nanorods

The optical properties of the gold nanorods in suspension were evaluated by Vis-NIR absorption spectroscopy using a Multiskan GO microplate spectrophotometer from Thermo Scientific. After attachment of the gold nanorods to the glass substrates, the optical properties of the samples were evaluated by recording the absorption spectra in air using a Hewlett Packard 8453 spectrophotometer. The gold nanorod surface attachment to the glass and titanium substrates was characterized using a Zeiss Ultra 55 scanning electron microscope. Imaging was performed in the secondary electron mode with an acceleration voltage of 2.5 kV for the glass and 5 kV for the titanium substrates. For one sample of each type, eight micrographs at 50,000× magnification were acquired at different locations spread across the sample surface. The surface coverage of gold nanorods (in percent) was quantified by image analysis of the SEM micrographs and expressed as the projected surface area covered by the gold nanorods. SEM was also used to visualize monolayers of *S. aureus* cells cultivated on solid-supported gold nanorods on titanium.

4.4. Thermal Imaging

Thermal imaging was performed using a Testo 871 s thermal imager to evaluate the heating of AuNR840 supported on glass upon irradiation with NIR light. The NIR laser used was acquired from BWT Beijing Ltd., model DS3-.00 W, with a central wavelength of 808 ± 3 nm. The laser fiber optic was connected to an air-spaced doublet collimator (F810SMA-780, Thorlabs) fitted with a 2X beam expander (GBE02-B, Thorlabs). The laser power output was measured using an optical power meter (PM160T-HP, Thorlabs), and the irradiance was calculated based on the measured beam area (details in the Supporting Information). AuNR840 and bare glass control samples (three replicates of each, $n = 3$) were placed on Mueller–Hinton (MH) agar

https://doi.org/10.1021/acsabm.6c00525
ACS Appl. Bio Mater. XXXX, XXX, XXX–XXX

plates, with the gold nanorods facing the agar. The laser collimator was positioned 10 cm above the agar plates, and the samples were irradiated for 30 s at an irradiance of 4.7 W cm^{-2}. Thermal images were recorded before and after irradiation.

4.5. In Vitro Antibacterial Activity Evaluation

The in vitro antibacterial activity was evaluated against *S. aureus* (CCUG 10778), using an agar plate model adapted from a previously published protocol.[9] Bare glass substrates were used as controls, and all samples used in the antibacterial activity evaluation were sterilized by exposure to UV light in a UV/O_3 cleaner for 5 min. *S. aureus* was inoculated in tryptic soy broth (TSB) and incubated at 37 °C until an optical density (OD) of 0.55, corresponding to 10^8 CFU ml^{-1} was reached. The suspension was then diluted to 7×10^4 CFU ml^{-1} with phosphate-buffered saline (PBS). A second suspension was prepared in the same manner, supplemented with 3.125 μM of the RRP9W4N AMP (RRPRPRPRPWWWW-NH_2, M_W = 1930 g mol^{-1}, purity > 90%, GenScript). The bacterial suspensions were streaked onto separate Mueller–Hinton agar plates using cotton swabs, and the samples were placed onto the plates with the functionalized side facing the bacteria. Relevant samples were irradiated with the NIR laser for 30 s at an irradiance of 4.7 W cm^{-2} for AuNR840, and 5.4 W cm^{-2} for AuNR870. A schematic illustration of the experimental setup is shown in Figure 5. The plates were incubated at 37 °C for 16 h, whereafter the number of bacterial colonies beneath each sample was quantified. Colonies appearing at the outermost 1 mm perimeter of the samples were excluded to avoid bacteria growing in from the edges to influence the results. The antibacterial efficacy, in percent, was determined as:

$$\text{Antibacterial efficacy} = \frac{A - B}{A} \times 100$$

where A is the number of colony-forming units per unit area (CFU cm^{-2}) of the control group and B is the number of colony-forming units per area of the test group. All sample groups were tested in triplicate, and experiments were repeated three times ($n = 9$). Data are expressed as mean CFU cm^{-2} values with standard deviation. Pairwise two-sample t-tests assuming unequal variance were used for statistical analysis. Significant differences in bar charts are indicated with letters. Groups sharing the same letter indicate that there is no statistically significant difference between the means, while groups with different letters indicate that there is a statistically significant difference between the means.

4.6. Interaction between Solid-Supported Gold Nanorods and *S. aureus*

Samples with AuNR870 supported on titanium were sterilized by exposure to UV light in a UV/O_3 cleaner for 5 min. A single colony of *S. aureus* (CCUG 10778) was inoculated in 4 mL of TSB and incubated at 37 °C until an OD of 0.55–0.70 was reached. The bacterial suspension was then washed by centrifugation at 4000 *g* for 5 min, whereafter 1 mL of the bacterial pellet was redispersed in PBS to a total volume of 5.5 mL. The bacterial inoculum was added to the AuNR870 samples and incubated at 37 °C for 30 min. After incubation, the samples were rinsed twice with 1 mL of PBS. Once *S. aureus* had been cultured on the AuNR870-functionalized titanium, the samples were fixated by immersion in 4% formaldehyde at 4 °C overnight (17–18 h). Thereafter, they were stepwise dehydrated in an ethanol gradient before being immersed in a 50 vol% solution of hexamethyldisilazane (HMDS) in ethanol for 15 min. Lastly, the samples were immersed in pure HMDS (99%) for 15 min, after which the liquid was removed, and the samples were allowed to dry. For SEM characterization, the fixated samples were sputter coated with a 5 nm gold layer. SEM imaging was conducted with the sample at an angle, using acceleration voltages between 3 and 5 kV. For transmission electron microscopy (TEM) investigation of the gold nanorod-bacteria interaction, the titanium samples were first sputter coated with a 100 nm protective chromium layer. TEM specimens were prepared following a conventional FIB-SEM lift-out protocol,[46,47] using a FEI Versa 3D system equipped with a mono-isotopic Ga (69 amu) ion source. A region of interest was identified that contained a sufficient number of bacterial cells to be included in the final specimen. A platinum strip, 2 × 10 μm, was deposited using the instrument's gas injection system, first by e-beam deposition, followed by ion beam deposition until a thickness of greater than 1 μM was obtained. Trenches were then milled around the platinum strip using a cleaning cross-section pattern, followed by a U-cut underneath the lamella. An Omniprobe micromanipulator was positioned onto the lamella and attached by platinum deposition. The lamella was cut loose and mounted onto a copper half-grid. It was subsequently polished using ion beam milling at 30 kV with progressively reduced currents from 100 to 10 pA, until it was sufficiently thin for TEM analysis (< 100 nm). A SEM micrograph of a TEM-ready lamella is shown in Figure S6. The TEM specimens were analyzed using an FEI Titan 80–300 operated at 300 kV and imaged in brightfield TEM-mode. Micrographs were analyzed using the Gatan Digital Micrograph 3 software.

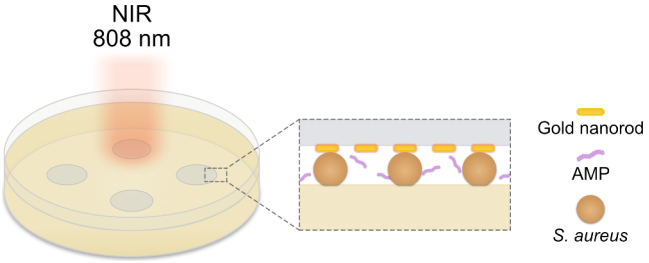

Figure 5. Schematic illustration of the agar plate model used in the in vitro antibacterial activity evaluation.

4.7. Bacterial Cytological Profiling

Sample preparation for bacterial cytological profiling was based on a modified version of the agar plate model employed in the in vitro antibacterial activity evaluation. All solid-supported gold nanorod samples used for BCP were prepared with AuNR840 and sterilized by exposure to UV light for 5 min prior to the experiments. *S. aureus* (CCUG 10778) was inoculated in TSB and incubated at 37 °C until reaching an OD of 0.6. From this bacterial culture, three separate suspensions were prepared by dilution with PBS to a final OD of 0.3: one untreated (negative control), one supplemented with 3.125 μM RRP9W4N AMP, and one supplemented with 10 μM nisin (positive control). The three suspensions were incubated for 10 min before being streaked onto separate MH agar plates. Two samples (AuNR840 supported on glass) were placed onto each agar plate with the nanorods facing the bacteria, and one sample per plate was subsequently irradiated at 4.7 W cm^{-2} for 30 s. The samples were then removed from the agar plates, and circular agar punches (8 mm diameter) were taken from the regions underneath each sample. Bacterial cells from the 8 mm punches were transferred by stamping to 1.2% agarose patches containing 10% MHB, DAPI (0.2 μg ml^{-1}), SytoxGreen (40 nM), FM4-64 (0.2 μg ml^{-1}), and $DiSC_35$ (0.1 μM) to ensure sufficient staining of the cells. The samples were sealed with poly-L-dopamine-coated coverslips[36] and immediately imaged using a Nikon Eclipse Ti2 microscope equipped with a Photometrics PRIME BSI camera, a CFI Plan Apochromat DM lambda 100× oil objective (N.A. 1.45, W.D. 0.13 mm), a Lumencor Sola SE II FISH 365 light source, and an Okolab temperature chamber set to 37 °C. Images were acquired using NIS elements AR software version 5.21.03. The BCP experiments were performed in three independent biological replicates.

4.8. Image Analysis of BCP

Fluorescence intensity parameters were analyzed using the ImageJ plugin MicrobeJ.[48,49] Cells were detected in phase contrast images using

https://doi.org/10.1021/acsabm.6c00525
ACS Appl. Bio Mater. XXXX, XXX, XXX–XXX

the fit shape detection mode with circular settings. The area parameter was adjusted to 0.2 to max, while all other parameters were kept at their default settings. Statistical analysis was performed using GraphPad Prism 10.6.1 as specified in the figure legends.

■ ASSOCIATED CONTENT

Supporting Information

The Supporting Information is available free of charge at https://pubs.acs.org/doi/10.1021/acsabm.6c00525.

Complementary experimental data, calculations, and details on the NIR laser power output; transmission electron microscopy micrograph of gold nanorods; thermal images of glass control (top) and AuNR840 (bottom) samples; antibacterial activity against *S. aureus* and representative images of the samples from the agar plate model; estimation on the number of gold nanorods in contact with a bacterial cell; quantification of normalized DAPI fluorescence intensity, normalized phase density, and cell area; NIR laser intensity; data on the NIR laser system's power output and the irradiance; relationship between the set NIR laser power (W) and the irradiance; TEM specimen preparation; and SEM micrograph of a TEM specimen from the FIB-SEM (PDF)

■ AUTHOR INFORMATION

Corresponding Author

Martin Andersson – *Department of Chemistry and Chemical Engineering, Chalmers University of Technology, Gothenburg 412 96, Sweden; Center for Antibiotic Resistance Research in Gothenburg (CARe), Gothenburg 413 46, Sweden;* orcid.org/0000-0003-1523-4697; Email: martin.andersson@chalmers.se

Authors

Maja Lidström Uusitalo – *Department of Chemistry and Chemical Engineering, Chalmers University of Technology, Gothenburg 412 96, Sweden; Center for Antibiotic Resistance Research in Gothenburg (CARe), Gothenburg 413 46, Sweden*

Alva Nilsson – *Department of Chemistry and Chemical Engineering, Chalmers University of Technology, Gothenburg 412 96, Sweden*

Ann-Britt Schäfer – *Division of Molecular Bioscience, Department of Life Sciences, Chalmers University of Technology, Gothenburg 412 96, Sweden; Center for Antibiotic Resistance Research in Gothenburg (CARe), Gothenburg 413 46, Sweden*

Gustav Eriksson – *Department of Chemistry and Chemical Engineering, Chalmers University of Technology, Gothenburg 412 96, Sweden;* orcid.org/0009-0001-2330-6227

Mats Hulander – *Department of Chemistry and Chemical Engineering, Chalmers University of Technology, Gothenburg 412 96, Sweden; Center for Antibiotic Resistance Research in Gothenburg (CARe), Gothenburg 413 46, Sweden;* orcid.org/0000-0003-2921-5438

Michaela Wenzel – *Division of Molecular Bioscience, Department of Life Sciences, Chalmers University of Technology, Gothenburg 412 96, Sweden; Center for Antibiotic Resistance Research in Gothenburg (CARe), Gothenburg 413 46, Sweden;* orcid.org/0000-0001-9969-6113

Complete contact information is available at: https://pubs.acs.org/doi/10.1021/acsabm.6c00525

Funding

The authors thank the Area of Advance in Materials Science at Chalmers University of Technology, Knut and Alice Wallenberg Foundation through the Wallenberg Academy Fellow program for the funding.

Notes

The authors declare no competing financial interest.

■ REFERENCES

(1) Høiby, N.; Bjarnsholt, T.; Givskov, M.; Molin, S.; Ciofu, O. Antibiotic Resistance of Bacterial Biofilms. *Int. J. Antimicrob. Agents* **2010**, *35*(4), 322–332.

(2) Murray, C. J.; Ikuta, K. S.; Sharara, F.; Naghavi, M. Global Burden of Bacterial Antimicrobial Resistance in 2019: A Systematic Analysis. *Lancet* **2022**, *399* (10325), 629–655.

(3) World Health Organization. *Global Antibiotic Resistance Surveillance Report 2025: WHO Global Antimicrobial Resistance and Use Surveillance System (GLASS)*; Geneva, **2025**.

(4) Campoccia, D.; Montanaro, L.; Arciola, C. R. A Review of the Biomaterials Technologies for Infection-Resistant Surfaces. *Biomaterials* **2013**, *34* (34), 8533–8554.

(5) Su, Q.; Xue, Y.; Wang, C.; Zhou, Q.; Zhao, Y.; Su, J.; Zhu, B. Strategies and Applications of Antibacterial Surface-Modified Biomaterials. *Bioact. Mater.* **2025**, *53*, 114–140.

(6) Doveri, L.; Diaz Fernandez, Y. A.; Dacarro, G. Nanomaterials for Photothermal Antimicrobial Surfaces. *ACS Omega* **2024**, *9* (24), 25575–25590.

(7) Feng, Z.; Tang, T.; Wu, T.; Yu, X.; Zhang, Y.; Wang, M.; Zheng, J.; Ying, Y.; Chen, S.; Zhou, J.; Fan, X.; Zhang, D.; Li, S.; Zhang, M.; Qian, J. Perfecting and Extending the Near-Infrared Imaging Window. *Light Sci. Appl.* **2021**, *10*, 197.

(8) Weissleder, R. A Clearer Vision for in Vivo Imaging. *Nat. Biotechnol.* **2001**, *19*, 316–317.

(9) Uusitalo, M.; Eriksson, G.; Hulander, M.; Andersson, M. Gold Nanorods as Photothermal Antibacterial Materials. *ACS Appl. Nano Mater.* **2025**, *8* (7), 3661–3670.

(10) Zhao, Y. Q.; Sun, Y.; Zhang, Y.; Ding, X.; Zhao, N.; Yu, B.; Zhao, H.; Duan, S.; Xu, F. J. Well-Defined Gold Nanorod/Polymer Hybrid Coating with Inherent Antifouling and Photothermal Bactericidal Properties for Treating an Infected Hernia. *ACS Nano* **2020**, *14* (2), 2265–2275.

(11) Miguel, I.De; Prieto, I.; Albornoz, A.; Sanz, V.; Weis, C.; Turon, P.; Quidant, R. Plasmon-Based Biofilm Inhibition on Surgical Implants. *Nano Lett.* **2019**, *19* (4), 2524–2529.

(12) Pihl, M.; Bruzell, E.; Andersson, M. Bacterial Biofilm Elimination Using Gold Nanorod Localised Surface Plasmon Resonance Generated Heat. *Mater. Sci. Eng. C Mater. Biol. Appl.* **2017**, *80*, 54–58.

(13) Huang, X.; Jain, P. K.; El-Sayed, I. H.; El-Sayed, M. A. Plasmonic Photothermal Therapy (PPTT) Using Gold Nanoparticles. *Lasers Med. Sci.* **2008**, *23* (3), 217–228.

(14) Yang, T.; Wang, D.; Liu, X. Assembled Gold Nanorods for the Photothermal Killing of Bacteria. *Colloids Surf., B* **2019**, *173*, 833–841.

(15) Zhao, Y.-Q.; Xiu, Z.; Wu, R.; Zhang, L.; Ding, X.; Zhao, N.; Duan, S.; Xu, F.-J. A Near-Infrared-Responsive Quaternary Ammonium/Gold Nanorod Hybrid Coating with Enhanced Antibacterial Properties. *Adv. NanoBiomed Res.* **2022**, *2* (11).

(16) Zimmerli, W.; Trampuz, A.; Ochsner, P. E. Prosthetic-Joint Infections. *N. Engl. J. Med.* **2004**, *351* (16), 1645–1654.

(17) Shai, Y. Mode of Action of Membrane Active Antimicrobial Peptides. *Biopolymers* **2002**, *66*, 236–248.

(18) Yeung, A. T. Y.; Gellatly, S. L.; Hancock, R. E. W. Multifunctional Cationic Host Defence Peptides and Their Clinical Applications. *Cell. Mol. Life Sci.* **2011**, *68* (13), 2161–2176.
(19) Xu, X.; Ding, Y.; Hadianamrei, R.; Lv, S.; You, R.; Pan, F.; Zhang, P.; Wang, N.; Zhao, X. Antimicrobial Peptide Functionalized Gold Nanorods Combining Near-Infrared Photothermal Therapy for Effective Wound Healing. *Colloids Surf., B* **2022**, 220.
(20) Chen, J.; Dai, T.; Yu, J.; Dai, X.; Chen, R.; Wu, J.; Li, N.; Fan, L.; Mao, Z.; Sheng, G.; Li, L. Integration of Antimicrobial Peptides and Gold Nanorods for Bimodal Antibacterial Applications. *Biomater. Sci.* **2020**, *8* (16), 4447–4457.
(21) Huang, X.; Xu, L.; Yu, X.; Li, Y.; Huang, Z.; Xu, R.; Zeng, W.; Zhang, Z.; Li, W.; Deng, F. Near-Infrared Light-Responsive Multifunctional Hydrogel Releasing Peptide-Functionalized Gold Nanorods Sequentially for Diabetic Wound Healing. *J. Colloid Interface Sci.* **2023**, *639*, 369–384.
(22) Sankari, S. S.; Dahms, H. U.; Tsai, M. F.; Lo, Y. L.; Wang, L. F. Comparative Study of an Antimicrobial Peptide and a Neuropeptide Conjugated with Gold Nanorods for the Targeted Photothermal Killing of Bacteria. *Colloids. Surf. B* **2021**, *208*, No. 112117.
(23) Moorcroft, S. C. T.; Roach, L.; Jayne, D. G.; Ong, Z. Y.; Ong, Z. Y.; Evans, S. D. Nanoparticle-Loaded Hydrogel for the Light-Activated Release and Photothermal Enhancement of Antimicrobial Peptides. *ACS Appl. Mater. Interfaces* **2020**, *12* (22), 24544–24554.
(24) Atefyekta, S.; Blomstrand, E.; Rajasekharan, A. K.; Svensson, S.; Trobos, M.; Hong, J.; Webster, T. J.; Thomsen, P.; Andersson, M. Antimicrobial Peptide-Functionalized Mesoporous Hydrogels. *ACS Biomater. Sci. Eng.* **2021**, *7* (4), 1693–1702.
(25) Stepulane, A.; Rajasekharan, A. K.; Andersson, M. Multifunctional Surface Modification of PDMS for Antibacterial Contact Killing and Drug-Delivery of Polar, Nonpolar, and Amphiphilic Drugs. *ACS Appl. Bio Mater.* **2022**, *5* (11), 5289–5301.
(26) Blomstrand, E.; Rajasekharan, A. K.; Atefyekta, S.; Andersson, M. Cross-Linked Lyotropic Liquid Crystal Particles Functionalized with Antimicrobial Peptides. *Int. J. Pharm.* **2022**, *627*, No. 122215.
(27) Blomstrand, E.; Atefyekta, S.; Rajasekharan, A. K.; Andersson, M. Clinical Investigation of Use of an Antimicrobial Peptide Hydrogel Wound Dressing on Intact Skin. *J. Wound Care* **2023**, *32* (6), 368–375.
(28) Stepulane, A.; Rajasekharan, A. K.; Andersson, M. Antibacterial Efficacy of Antimicrobial Peptide-Functionalized Hydrogel Particles Combined with Vancomycin and Oxacillin Antibiotics. *Int. J. Pharm.* **2024**, *664*, No. 124630.
(29) Schäfer, A.-B.; Sidarta, M.; Abdelmesseh Nekhala, I.; Marinho Righetto, G.; Arshad, A.; Wenzel, M. Dissecting Antibiotic Effects on the Cell Envelope Using Bacterial Cytological Profiling: A Phenotypic Analysis Starter Kit. *Microbiol. Spectr.* **2024**, *12* (3), No. e0327523.
(30) Uusitalo, M.; Strach, M.; Eriksson, G.; Dmytrenko, T.; Andersson, J.; Dahlin, A.; Hulander, M.; Andersson, M. Photothermal Properties of Solid-Supported Gold Nanorods. *Nano Lett.* **2024**, *24* (40), 12529–12535.
(31) Lidström Uusitalo, M.; Strach, M.; Hulander, M.; Andersson, M. Gold Nanorod Gradient Surfaces. *Appl. Surf. Sci.* **2026**, *729*, No. 166104.
(32) Blomstrand, E.; Posch, E.; Stepulane, A.; Rajasekharan, A. K.; Andersson, M. Antibacterial and Hemolytic Activity of Antimicrobial Hydrogels Utilizing Immobilized Antimicrobial Peptides. *Int. J. Mol. Sci.* **2024**, *25* (8), 4200.
(33) Golding, C. G.; Lamboo, L. L.; Beniac, D. R.; Booth, T. F. The Scanning Electron Microscope in Microbiology and Diagnosis of Infectious Disease. *Sci. Rep.* **2016**, *6*, 26516.
(34) Nonejuie, P.; Burkart, M.; Pogliano, K.; Pogliano, J. Bacterial Cytological Profiling Rapidly Identifies the Cellular Pathways Targeted by Antibacterial Molecules. *Proc. Natl. Acad. Sci. U. S. A.* **2013**, *110* (40), 16169–16174.
(35) Buttress, J. A.; Schäfer, A.-B.; Koh, A.; Wheatley, J.; Mickiewicz, K.; Wenzel, M.; Strahl, H. The Last Resort Antibiotic Daptomycin Exhibits Two Independent Antibacterial Mechanisms of Action. *bioRxiv* **2024**, No. 629673.
(36) Te Winkel, J. D.; Gray, D. A.; Seistrup, K. H.; Hamoen, L. W.; Strahl, H. Analysis of Antimicrobial-Triggered Membrane Depolarization Using Voltage Sensitive Dyes. *Front. Cell Dev. Biol.* **2016**, *4*, 29.
(37) Hover, B. M.; Kim, S.-H.; Katz, M.; Charlop-Powers, Z.; Owen, J. G.; Ternei, M. A.; Maniko, J.; Estrela, A. B.; Molina, H.; Park, S.; Perlin, D. S.; Brady, S. F. Culture-Independent Discovery of the Malacidins as Calcium-Dependent Antibiotics with Activity against Multidrug-Resistant Gram-Positive Pathogens. *Nat. Microbiol.* **2018**, *3* (4), 415–422.
(38) Pogliano, J.; Pogliano, N.; Silverman, J. A. Daptomycin-Mediated Reorganization of Membrane Architecture Causes Mislocalization of Essential Cell Division Proteins. *J. Bacteriol.* **2012**, *194* (17), 4494–4504.
(39) Malmsten, M.; Kasetty, G.; Pasupuleti, M.; Alenfall, J.; Schmidtchen, A. Highly Selective End-Tagged Antimicrobial Peptides Derived from PRELP. *PLoS. One* **2011**, *6* (1), No. e16400.
(40) Schäfer, A.-B.; Steenhuis, M.; Jim, K. K.; Neef, J.; O'Keefe, S.; Whitehead, R. C.; Swanton, E.; Wang, B.; Halbedel, S.; High, S.; Dijl, J. M.van; Luirink, J.; Wenzel, M. Dual Action of Eeyarestatin 24 on Sec-Dependent Protein Secretion and Bacterial DNA. *ACS Infect. Dis.* **2023**, *9* (2), 253–269.
(41) Özsan, Ç.; Schäfer, A.-B.; Akhir, A.; Aning, O. A.; Fulgencio, S.; Maitra, R.; Rani, R.; Saxena, D.; Westerlund, F.; Chopra, S.; Wenzel, M.; Frei, A. A Platinum Butterfly Effect: Small Changes Turn an Anticancer Drug into a Non-Toxic Metalloantibiotic with In Vivo Efficacy. *bioRxiv* **2025**No. 657029.
(42) Sean Norman, R.; Stone, J. W.; Gole, A.; Murphy, C. J.; Sabo-Attwood, T. L. Targeted Photothermal Lysis of the Pathogenic Bacteria, Pseudomonas Aeruginosa, with Gold Nanorods. *Nano Lett.* **2008**, *8* (1), 302–306.
(43) Zhao, Y.; Guo, Q.; Dai, X.; Wei, X.; Yu, Y.; Chen, X.; Li, C.; Cao, Z.; Zhang, X. A Biomimetic Non-Antibiotic Approach to Eradicate Drug-Resistant Infections. *Adv. Mater.* **2019**, *31* (7), No. 1806024.
(44) Scarabelli, L.; Sánchez-Iglesias, A.; Pérez-Juste, J.; Liz-Marzán, L. M. A "Tips and Tricks" Practical Guide to the Synthesis of Gold Nanorods. *J. Phys. Chem. Lett.* **2015**, *6* (21), 4270–4279.
(45) Ferhan, A. R.; Guo, L.; Kim, D. H. Influence of Ionic Strength and Surfactant Concentration on Electrostatic Surfacial Assembly of Cetyltrimethylammonium Bromide-Capped Gold Nanorods on Fully Immersed Glass. *Langmuir* **2010**, *26* (14), 12433–12442.
(46) Giannuzzi, L. A.; Stevie, F. A. A Review of Focused Ion Beam Milling Techniques for TEM Specimen Preparation. *Micron* **1999**, *30* (3), 197–204.
(47) Langford, R. M.; Clinton, C. In Situ Lift-out Using a FIB-SEM System. *Micron* **2004**, *35* (7), 607–611.
(48) Schindelin, J.; Arganda-Carreras, I.; Frise, E.; Kaynig, V.; Longair, M.; Pietzsch, T.; Preibisch, S.; Rueden, C.; Saalfeld, S.; Schmid, B.; Tinevez, J.-Y.; White, D. J.; Hartenstein, V.; Eliceiri, K.; Tomancak, P.; Cardona, A. Fiji: An Open-Source Platform for Biological-Image Analysis. *Nat. Methods* **2012**, *9* (7), 676–682.
(49) Ducret, A.; Quardokus, E. M.; Brun, Y. V. MicrobeJ, a Tool for High Throughput Bacterial Cell Detection and Quantitative Analysis. *Nat. Microbiol.* **2016**, *1* (7), 16077.

https://doi.org/10.1021/acsabm.6c00525
ACS Appl. Bio Mater. XXXX, XXX, XXX–XXX